Wind Energy

WILEY

RESEARCH ARTICLE OPEN ACCESS

Assessing the Underwater Impact of Aerodynamic Noise From Offshore Wind Turbines

Laura Botero-Bolívar[1] | Oscar A. Marino Sánchez[2] | Martín de Frutos[2] | Esteban Ferrer[2]

[1]Mechanical Engineering Department, Universidad Industrial de Santander, Bucaramanga, Colombia | [2]ETSIAE-UPM, School of Aeronautics, Universidad Politécnica de Madrid, Madrid, Spain

Correspondence: Esteban Ferrer (esteban.ferrer@upm.es)

Received: 22 September 2025 | **Revised:** 8 May 2026 | **Accepted:** 23 May 2026

ABSTRACT

The growing demand for offshore wind energy has led to a significant increase in wind turbine size and to the development of large-scale wind farms, often comprising 100–150 turbines. However, the environmental impact of underwater noise emissions remains largely unaddressed. This paper quantifies, for the first time, the underwater aerodynamic noise footprint of three large offshore turbines (5, 10, and 22 MW) and wind farms composed of these turbines. We propose a novel methodology that integrates validated wind turbine noise generation (i.e., blade element momentum theory and Amiet) with plane wave propagation theory in different media, enabling turbine designers to predict underwater noise emissions. Our results indicate that the three turbines generate underwater noise levels that exceed the hearing thresholds of the low-frequency hearing group in the range of 0.1–1 kHz. When scaled to represent wind farm conditions, the predicted noise levels may become detectable by additional hearing groups at frequencies up to 10 kHz. For the scenarios considered, the results suggest that aerodynamic noise from offshore wind farms could contribute to the underwater soundscape and may have implications for marine organisms. These findings highlight the importance of considering aerodynamic noise in environmental assessments of offshore wind energy development.

1 | Introduction

Anthropogenic underwater noise significantly impacts marine ecosystems, posing a natural equilibrium between different species [1]. Marine mammals are especially vulnerable to noise because they rely on sound to communicate, navigate, reproduce, feed, among other sensory purposes. A commonly cited problem concerning underwater noise is the masking problem [2], where anthropogenic noise can mask the natural sound present in marine environments, leading to alteration of behavior, reduction of communication ranges, foraging, predator and habitat avoidance [3, 4]. Furthermore, the propagation of sound in the sea is enhanced by the higher speed of sound in water than in air (1480 m/s for water vs. 343 m/s for air) and the lower attenuation of sound in water (0.1 dB/km in seawater vs. 5 dB/km for air at 1 kHz). These physical factors, together with the channeling of sound in shallow waters, make anthropogenic noise more critical underwater. For example, [5] measured underwater noise 20 km from a small offshore wind farm composed of only 16 wind turbines. Therefore, predicting underwater noise produced by offshore energy devices is paramount to guarantee sustainable exploitation of energy sources.

Wind turbine design for offshore environments has focused primarily on maximizing energy production (e.g., [6–8]), with limited attention given to the acoustic footprint and its environmental impact. Specifically, the underwater aerodynamic noise generated by offshore wind turbines has not yet been quantified, which is the focus of this work.

The aerodynamic noise of wind turbines is caused by the interaction between the turbulent wind and the turbine blades. Thus, it depends on the operational conditions and the size of the wind turbines (i.e., the tip speed and rotor area)—the overall sound pressure level of a wind turbine scales with the fifth power with the diameter of the wind turbine rotor. In recent years, the size

of offshore wind turbines has increased steadily in response to the growing demand for clean energy production. For example, the offshore wind turbine proposed within the IEA Task 55-REFWIND would produce 22-MW power with a rotor diameter of 284 m [9] and the recently announced MySE 22-MW offshore turbine from Mingyang Smart Energy with a rotor of 310+ m [10]. In addition, we face a rapid increase in the number of turbines gathered in farms. Today, the largest offshore wind farms (e.g., London Array, Gemini, Hornsea Project One and Two [11]) include more than 150 turbines. Simple acoustics shows that the noise produced by a wind farm of N wind turbines scales with the factor $20\log_{10}(N)$. The combination of increasingly large turbines gathered in farms with hundreds of turbines, combined with the negative impact of underwater noise, motivates this research: Can aerodynamic noise from offshore wind turbines affect marine life? To quantify this issue, we develop a new approach that combines wind turbine noise prediction techniques with wave theory to calculate the effective noise that penetrates underwater (due to change of media).

Wind turbine noise may be classified as mechanical and aerodynamic acoustic noise. The first type has a defined tonal character and is produced by mechanical components such as the gearbox and bearings (and/or generator or cooling systems) located within the device nacelle and may be controlled/minimized by appropriate insulation of the nacelle. The second type is more complex and is caused by the interaction of the blades moving through the air. Previous studies on offshore wind turbine noise have only considered mechanical noise and structure-borne aerodynamic noise, as they are directly propagated into the water through the vibrating tower (or platform) [5, 12–16].

A common justification for ignoring the aerodynamic noise (produced by the rotating blades) of offshore wind turbines is based on Snell's law [17], which states that only one portion of the noise produced in the air propagates into the water. For air–water interfaces, Snell states that only sound waves within a cone of 13° angle with respect to the air–water interface normal vector can propagate into the water; see Figure 3. This fact considerably limits the propagation of airborne noise sources into the water. Furthermore, the higher acoustic impedance of water compared to air (i.e., the acoustic impedance of water is 3600 times higher than the air's) leads to a high attenuation of the sound waves when entering water. The main contribution of this work is the development of a methodology to predict underwater aerodynamic noise from offshore wind turbines. The approach couples established aerodynamic noise prediction methods with plane wave theory and Snell's law to estimate sound transmission across the air-sea interface. The results suggest that aerodynamic noise from different turbine models may be detectable by several groups of marine animals, depending on frequency and source characteristics. This framework provides a tool to account for aerodynamic noise generation in turbine design and environmental assessments. Furthermore, the method offers a fast turnaround suitable for low-fidelity models, while remaining compatible with higher-fidelity approaches for improved characterization of the noise source and propagation.

Using the proposed approach, we will quantify how the underwater footprint of large offshore turbines can affect several marine species. We compute the aerodynamic noise of offshore wind turbines 5, 10, and 22 MW and compare the sound transmitted underwater to the hearing thresholds of many marine animals. We confirm that these emissions are an environmental problem that is exacerbated when large offshore farms with hundreds of turbines are built.

The remainder of the paper is organized as follows. Section 2 presents the methodology used in the research, including wind turbine noise prediction, modeling of the air–water interface, and the characteristics of the wind turbine models. Section 3 discusses the results and discussion. Finally, Section 4 shows the main conclusions of this research.

2 | Methodology

2.1 | Wind Turbine Noise Predictions

Aerodynamic noise, caused by the interaction of the flow with the structure, is the main source of noise of modern wind turbines [18]. Figure 1 sketches the typical aerodynamic environment and the sources of noise of an offshore wind turbine. The atmospheric turbulence interacts with the leading edge of the rotating blades, causing a low-frequency noise, known as leading edge (LE) noise. Additionally, the turbulent boundary layer on the blades that interacts with the finite trailing edge causes mid- to high-frequency noise, referred to as trailing edge (TE) noise. Overall, the wide range of turbulent scales—from hundreds of meters in atmospheric flow to millimeters in boundary layer flow—encountered by the wind turbine blades cause

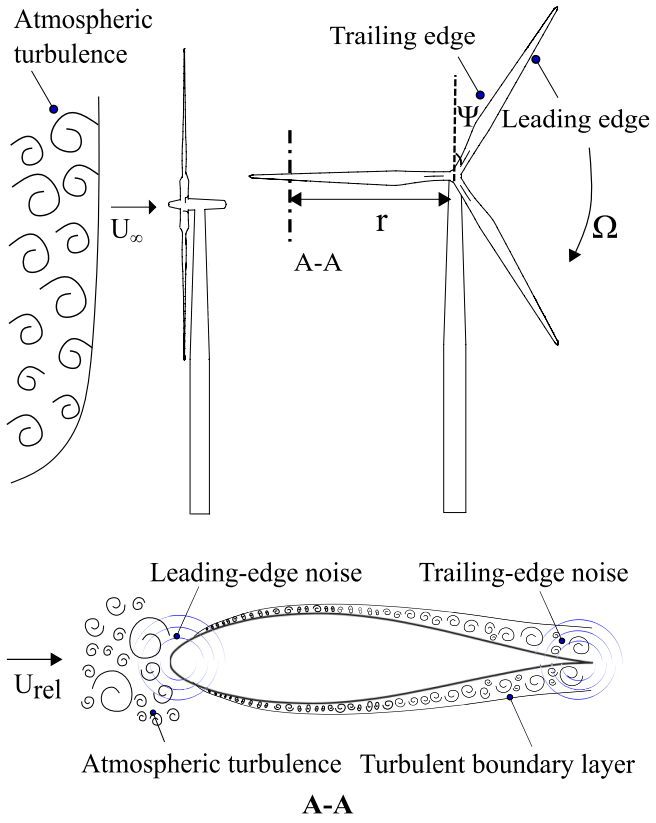

FIGURE 1 | Leading- and trailing-edge noise for an offshore wind turbine.

aerodynamic noise to exhibit a broadband nature, covering a wide range of frequencies. This is particularly critical for marine environments, as it can affect a variety of marine species with different hearing thresholds.

To compute the total aerodynamic noise of the wind turbine, we follow the method proposed by Schlinker-Amiet [19] for rotatory noise sources. We consider the strip theory approach, where the blade is divided into n segments. Each segment is considered as a 2D airfoil (as shown in the A-A cut in Figure 1). For each segment, leading- and trailing-edge noise ($S_{pp|\mathrm{LE}}$ and $S_{pp|\mathrm{TE}}$) are calculated as uncorrelated noise sources, such as $S_{pp|seg} = S_{pp|\mathrm{LE}} + S_{pp|\mathrm{TE}}$.

Leading- and trailing-edge noise (LE and TE) is predicted using Amiet's theory [20, 21] and the extension of [22] to consider the backscattering effect caused by airfoils of finite chords. The blade is divided into segments that are more refined near the tip of the blade, which is the part that generates most of the noise. An initial sinusoidal distribution of the location of the segments is proposed. The sinusoidal distribution is obtained by the horizontal coordinates of a point located in a semicircle of a diameter equal to the rotor radius (neglecting the inner part of the blades that consist of cylinders). The angle between the points on the radial axis was constant. After an iterative process to ensure that the aspect ratio (AR), defined as the span-chord ratio of the blade section, is greater than three, the radial position and the span and chord length distribution are obtained. The $AR \geq 3$ condition is adopted to satisfy the far-field condition assumed in Amiet's theory.

The von Kármán model [23] calculates the inflow turbulence spectrum used as input for predicting LE noise and an extension of the TNO-Blake model [24] computes the wall pressure spectrum to calculate trailing-edge noise. The boundary layer characteristics used as input in the TNO-Blake model are computed by XFOIL [25] using the flow conditions (angle of attack, α and relative velocity, U_{rel}) obtained with the blade element momentum theory (BEMT). The transition for XFOIL simulations was fixed at 5% of the chord. BEMT solutions are obtained using the open-source code OpenFAST [26], which includes the Prandlt tip and root loss correction factors and the Pitt/Peters skewed wake correction model.

Let us note that the methodology proposed in this work to link aerodynamic quantities to acoustic predictions is flexible and general in terms of flow conditions and wind turbine sizes. Indeed, the methods that we consider, that is, Amiet's theory for predicting the noise and the TNO-Blake model for calculating the wall-pressure spectrum are semi-analytical, meaning that they are based on theoretical considerations (and not data fitting). Furthermore, 2D section-based noise prediction methods in combination with BEMT are commonly applied for estimating blade noise in large wind turbines [27–32], including turbines of 5 MW [28] and 10 MW [32] providing quantitatively accurate results. In these predictions, the viscous/inviscid panel code XFOIL accounts for the Reynolds number and Mach number in the parameters of the boundary layer and therefore the acoustic quantities are appropriately calculated given the Reynolds number sectional. The resulting method is capable of predicting the noise spectra of wind turbine of any size.

The relative motion of the segment with respect to a fixed observer, due to the rotation of the blades, induces a delay between the noise emission and the location of the observer. This delay is quantified by a Doppler factor ($(\omega_e/\omega)^2$) which is incorporated into the prediction method as the squared ratio between the emitted frequency (ω_e) and the received frequency (ω). Subsequently, the total blade noise is calculated as the sum of all segments, calculated at every azimuth angle (Ψ in Figure 1):

$$S_{pp|\mathrm{blade}}(\omega, \Psi) = \sum_{1}^{n} S_{pp|\mathrm{seg}}(\omega_e, \Psi)(\omega_e/\omega)^2. \tag{1}$$

The average noise produced by the wind turbine in one rotation ($S_{pp|\mathrm{WT}}(\omega)$) is then calculated as

$$S_{pp|\mathrm{WT}}(\omega) = \frac{B}{2\pi} \int_{0}^{2\pi} S_{pp|\mathrm{blade}}(\omega, \Psi)\mathrm{d}\Psi, \tag{2}$$

where B is the number of blades. More information on the noise prediction methodology can be found in [31].

Appendix D presents the validation of the noise prediction methodology used in this investigation by comparing the predicted far-field noise with field measurements of a single Siemens 2.3-MW wind turbine. Furthermore, this methodology has been compared with others in [33]. We can conclude that the noise prediction methodology is validated and appropriate for the analyses carried out in this investigation.

To compute the noise generated by a wind farm, we assume that each turbine acts as an uncorrelated noise source with equal intensity; that is, the wake interaction between the turbines is not considered. We consider a squared layout with the turbines separated 4.5 diameters in the wind and transverse directions. The observer used to calculate the wind farm noise is located 100 m downstream of the last turbine and 10 m underwater; see Figure 2. It is important to note that wind farm noise is highly dependent on the observer's location and wind farm layout,

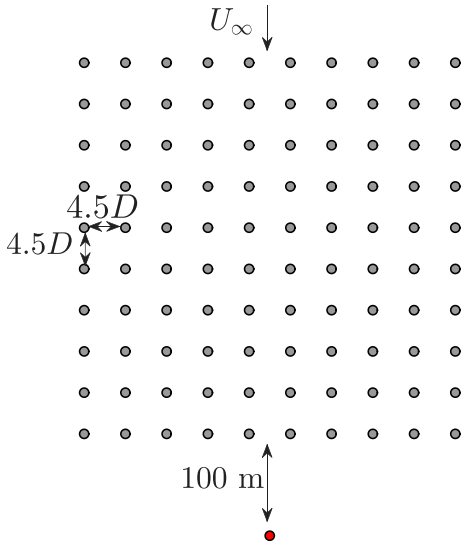

FIGURE 2 | Offshore wind farm layout.

since the distances between each turbine and the observer are huge. A more accurate assessment of a particular site can be obtained by detailing the exact wind farm layout and the particular positions of the observers.

2.2 | Air–Water Interface Modeling

The noise is calculated at two observers downstream of the turbine, as shown in Figure 3 left. The Air-side observer is located exactly at the air–water interface and the Water-side observer is located at 10 m depth from the air–water interface, both at a specific downstream position that is defined for each case analyzed in the results. Here, we pay particular attention to the propagation of noise underwater; therefore, additional steps need to be considered for the Water-side observer compared to the Air-side observer.

For the Air-side observer, the far-field noise is calculated directly at the observer, following the standard procedure of wind turbine noise prediction [31]. However, for the Water-side observer, the far-field noise cannot be computed directly at the observer because of the change of media that causes refraction and attenuation of the sound waves. This means that for each noise source (LE and TE of each segment at each azimuth location), only the direction of the sound waves that refracted at the air–water interface reaches the Water-side observer is considered. The rest of this subsection will address the details for the computation of the underwater noise. Furthermore, the algorithm with the methodology to compute the far-field noise spectrum at any Water-side observer is shown in Appendix B.

The refraction of the sound waves due to the change of medium is computed following Snell's law that establishes:

$$c_w \sin \Phi = c_a \sin \theta; \tag{3}$$

where c_w and c_a are the speed of sound in water and air, respectively, and Φ and θ are the angles formed by the sound wave and an axis perpendicular to the air–water interface in air and water, respectively, as shown in Figure 3 right. In this research, we consider a flat air–water interface. Non-flat air–water interfaces, caused for instance by sea-waves, would change the direction of the emitted noise but would not change the attenuation suffered by the air–water interface (see Appendix C for a discussion on this topic). Furthermore, if a specific sea state is known, the methodology proposed in this study can be applied to predict underwater noise. Φ is calculated for each blade segment at each azimuth location, considering the location of the noise source (segment noise) and the observer on the water side. With Φ defined, an observer *in the interface* is defined for each noise source, located at the intersection of the vector that connects the air–water interface with the noise source (following the angle Φ) and the air–water interface, as shown in Figure 3 right. The procedure to calculate ϕ and θ is shown in Appendix A. The far-field noise of each segment is then first calculated at the interface observer following the noise prediction approach for a single

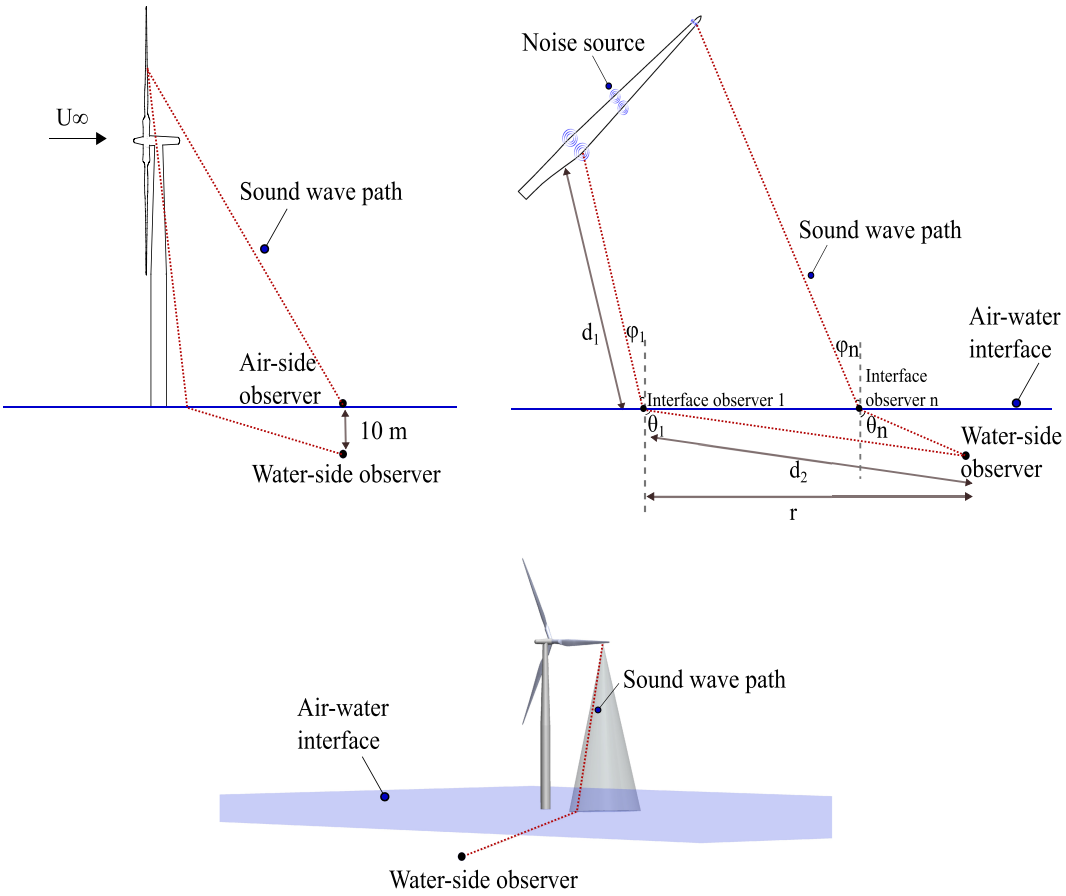

FIGURE 3 | Sketch of wind turbine noise trajectories for Air-side and Water-side observers. The lower figure shows the Snell cone delimiting the pressure waves that penetrate underwater.

medium (i.e., Amiet's theory for LE and TE noise). Subsequently, the noise is propagated from this interface observer to the Water-side observer through the water media. The blade noise, that is, the sum of all the segments, and the full wind turbine noise over the rotation, is calculated at the water-side observer.

The transmission coefficient of the acoustic pressure across the air–water interface is calculated for the plane wave theory as defined by [34]

$$T_{a\to w} = \frac{2\cos(\Phi)}{(\cos(\Phi) + gn\cos(\theta))}; \tag{4}$$

with Φ and θ calculated with the Snell's law, mentioned previously, g the ratio of densities and n the ratio of speed of sound of both media. $gn \approx 1/3600$ for the air–water case. $T_{a\to w}$ tends to 2, when Φ converges to ≈13°.

According to the literature, spherical waves can be approximated by plane waves for long distances, that is, at least 10 times the wavelength [17, 34–36]. This condition is verified for the turbines analyzed in this research. Figure 4 shows the ratio of distance from the noise source (each segment of the blade at each azimuth location) and wavelength for the NREL 5-MW and the EIA 22-MW turbines at $f = 100$ Hz and $f = 50$ Hz, respectively. The frequency analyzed is different for the turbines, as these are the minimum frequencies for each turbine where the wind turbine noise is relevant compared to the hearing threshold of marine animals (see Figure 5). For both turbines and all the segments, the condition of long distance (10 times the wavelength) is met, and hence, considering plane waves is an accurate approximation in this context. Furthermore, Appendix C includes a deeper discussion of calculating the transmission loss using spherical wave propagation and the effect on the prediction of far-field noise. Specifically, Figure C2 shows that there is no difference in the underwater noise spectrum when calculating the transmission loss using spherical and plane wave theories.

The propagation from the interface observer to the Water-side observer is obtained using the classic formulation of [37], which considers that most of the sound energy that is transmitted to the water by the acoustic ray limited by the Snell's law. For an observer that is directly under the noise source, the noise underwater appears to come from a virtual noise source at $h' = hc_a/c_w$, where h is the source height.

For observers not located directly beneath the source, the transmitted field can still be interpreted in terms of a virtual source; however, its apparent position is shifted both downward and laterally as a function of the refraction angle (θ_w). Based on this framework, [37] derived an expression for the ratio of acoustic pressure between the water-side observer and the interface observer, which can be written as

$$p_a/p_w = \frac{T_{a\to w} d_1}{\left(h + \frac{c_w d}{B^3 c_1}\right)^{1/2}\left(h + \frac{c_w d}{B c_1}\right)^{1/2}}; \tag{5}$$

where d is the observer's depth and $B = \cos(\theta)/\cos(\Phi)$. The transmission loss from the interface observer to the underwater observer is defined as $TL_{water} = 20\log_{10}(|p_a/p_w|)$. For wind farm cases, the underwater propagation distance between the noise source and the receiver can be large. Therefore, a cylindrical spreading model—commonly applied in shallow-water acoustics—is coupled to the present framework [38]. In this procedure, the sound level is first calculated at the receiver location to account for the appropriate emission and refraction angles. Then it is rescaled to a reference radial distance of 100 m and subsequently propagated from that point to the receiver, assuming cylindrical spreading.

The attenuation in the propagating medium (A) is considered for both media, air and water, as follows:

$$A = \alpha_a r_{\text{air/water}}; \tag{6}$$

where α is the attenuation in dB/m for each media and $r_{\text{air/water}}$ is the distance from the noise source to the underwater observer for each medium, that is, r_{air} for air is the linear distance from the noise source to the observer (d_1 in Figure 3), and for the

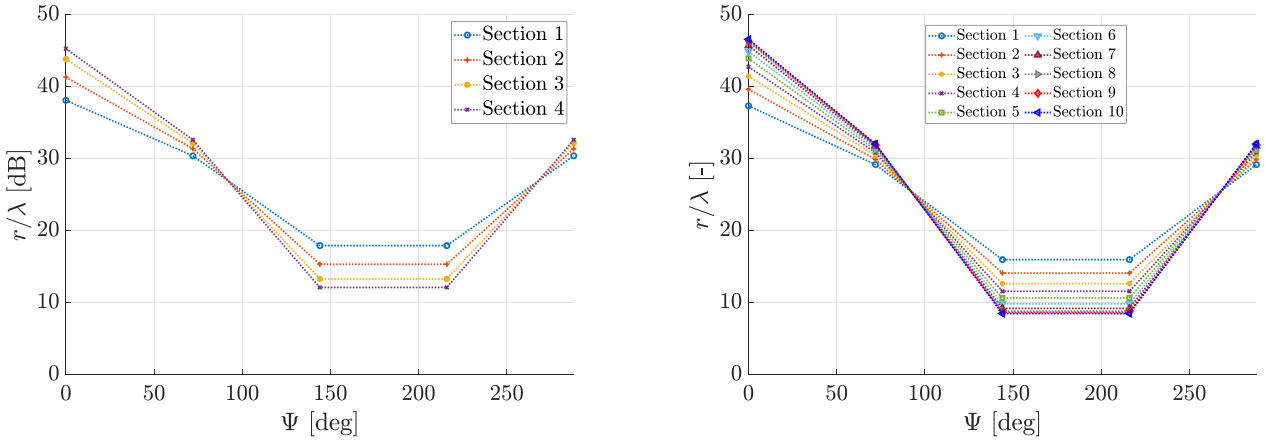

(a) NREL 5 MW. $f = 100$ Hz.

(b) IEA 22 MW. $f = 50$ Hz.

FIGURE 4 | r/λ for every blade section at each azimuth location. r is the distance of the noise source to the air–water interface (d_1 in Figure 3) and $\lambda = c/f$ is the wavelength. (a) NREL 5 MW. $f = 100$ Hz. (b) IEA 22 MW. $f = 50$ Hz.

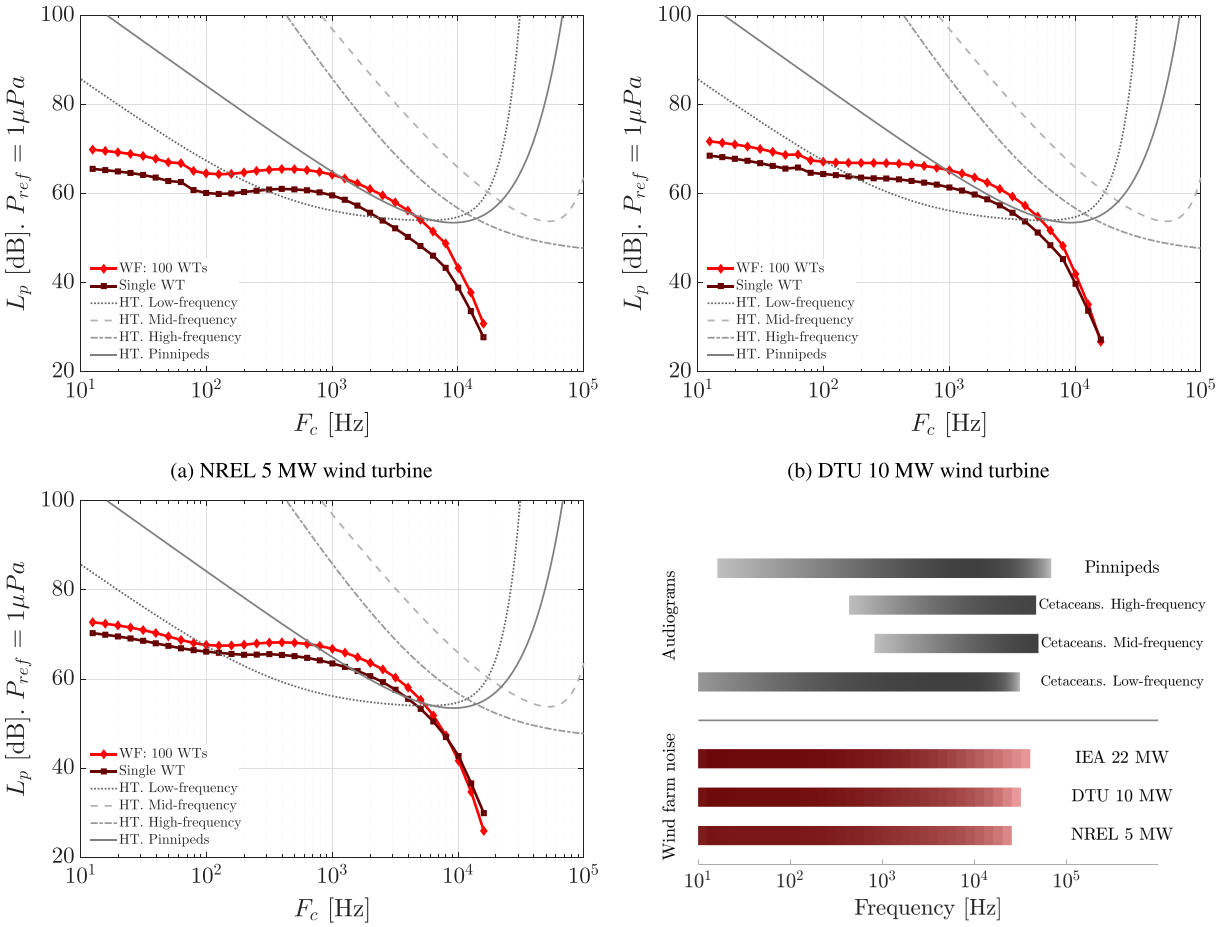

(a) NREL 5 MW wind turbine

(b) DTU 10 MW wind turbine

(c) IEA 22 MW wind turbine

(d) Overlap of wind farm noise (100 WT) and marine animals' audiograms

FIGURE 5 | One-third octave far-field noise spectra for a Water-side observer (10 m deep) at 100 m downwind the turbine compared to the hearing threshold of several groups of marine animals. L_p: sound pressure level; F_c: centered frequency; P_{ref}: reference pressure to convert to logarithmic scale; WT: wind turbine; WF: wind farm with 100; HT: hearing threshold. Color scales from 20 to 100 dB in (d). The observer for the wind farm is 100 m downstream the last turbine at the center of the turbine's array. (a) NREL 5-MW wind turbine. (b) DTU 10-MW wind turbine. (c) IEA 22-MW wind turbine. (d) Overlap of wind farm noise (100 WT) and marine animals' audiograms.

Water-side observer, r_{water} is the distance from the interface to the underwater observer (d_2 in Figure 3).

α for air (α_a) is calculated as the attenuation of a pure tone sound wave due to travel through the atmosphere. It is calculated using the standard ANSI/ASA S1.26 [36, 39]. The atmospheric conditions used in this research for the calculation of atmospheric attenuation is: $T = 15°C$ and $T_{\text{ref}} = 20°C$; $P = 98$ kPa and $P_{\text{ref}} = 101.325$ kPa; and $w = 86\%$; where T and T_{ref} are the source and reference temperatures, P and P_{ref} are the source and reference atmospheric pressures, and w is the relative humidity. α for water (α_w) is the sea-water attenuation in dB/m, calculated as proposed by [40], $P = 2$ atm (typical pressure at 10 m underwater), and $T = 8°C$ (typical conditions for sea-water).

To summarize, the sound pressure level at the underwater observer is calculated as

$$S_{pp_w}[dB] = 10\log_{10}(S_{pp,\text{interface}}) + TL_{water} - \alpha_a d_1 - \alpha_w d_2; \quad (7)$$

where $S_{pp,\text{interface}}$ denotes the sound pressure spectrum predicted using Amiet's theory at an observer located at the air–water interface (see Figure 3). For the wind farm case, cylindrical spreading is accounted for by including an additional term $10\log_{10}(r/r_{\text{ref}})$, where $r_{\text{ref}} = 100$ m and r is the horizontal distance between the underwater observer and the point in the interface where the sound wave impinges the water, that is, the interface observer (see Figure 3).

2.3 | Offshore Wind Turbine Models

In our study, we consider three offshore wind turbines that span a wide range of geometric and operational conditions, to consider the effect of size on aerodynamic noise and the impact on marine life: the NREL 5 MW [41], the DTU 10 MW [42], and the IEA 22 MW [9, 43]. Table 1 summarizes the geometrical details and nominal operational conditions of the turbines. We assume a turbulence intensity of 9% and an integral length scale of 100 m for all cases, since these are typical values for offshore

TABLE 1 | Geometrical and operational (nominal) conditions of three large offshore wind turbines.

Characteristic	NREL 5 MW	DTU 10 MW	IEA 22 MW
Hub height (m)	90.0	119.0	170.0
Rotor diameter (m)	126.0	178.4	284.0
Nominal wind velocity (m/s)	11.4	11.4	11.13
Rotor angular velocity (rpm)	12.1	9.6	6.85
Blade tip velocity (m/s)	79.0	90.0	101.92
Blade pitch (deg.)	0.0	0.0	4.12

TABLE 2 | Parameters for the composite audiograms of marine mammal functional hearing groups [48].

Hearing group	T_0	A	B	F_1 (kHz)	F_2 (kHz)	TTS (dB 1 μPa)	PTS (dB 1 μPa)
LF cetaceans	53.19	20.0	3.2	0.412	9.4	177	197
MF cetaceans	46.2	35.5	3.56	25.9	47.8	181	201
HF cetaceans	46.4	42.3	17.1	7.57	126	161	181
Phocid pinnipeds	43.7	20.1	1.41	10.2	3.97	175	195

sites [44, 45]. Those values are used to compute the von Kármán spectrum to predict LE noise. The effect of turbulence intensity is also discussed in the results section.

2.4 | Hearing Thresholds and Functional Hearing Groups

Marine mammal auditory sensitivity is represented using composite audiograms defined for functional hearing groups, following the framework proposed by [46, 47] and adopted in the NMFS Technical Guidance [48]. The parametric formulation is based on multiple behavioral and auditory evoked potential (AEP) measurement campaigns conducted across different laboratories and species. These composite curves represent best-fit envelope functions to aggregated datasets rather than single-species audiograms.

The underlying experimental database includes classical behavioral threshold studies such as bottlenose dolphin measurements by [49], harbor porpoise audiograms by [50], harbor seal measurements by [51] and [52], and masked threshold and temporary threshold shift experiments reported by [53] and [54]. Broader syntheses and discussions of masking and hearing variability are provided in [2]. The composite audiograms are described by the following functional form [48]:

$$T(f) = T_0 + A\log_{10}\left(1 + \frac{F_1}{f}\right) + \left(\frac{f}{F_2}\right)^B, \tag{8}$$

where $T(f)$ is the hearing threshold (dB re 1 μPa), f is the frequency (kHz), T_0 is the minimum threshold level, A and B control the low- and high-frequency slopes, and F_1 and F_2 define the transition frequencies of the U-shaped curve. Here, we consider four hearing functional groups, that is, low-frequency cetacean (LF), mid-frequency cetaceans (MF), high-frequency cetaceans (HF), and Phocid pinnipeds (PW). The parameters to calculate the audiogram of the groups of interest are shown in Table 2.

TABLE 3 | Parameters for the weighting function [48].

Hearing group	C	a	b	f_1 (kHz)	f_2 (kHz)
LF cetaceans	0.13	1	2	0.2	19
MF cetaceans	1.20	1.6	2	8.8	110
HF cetaceans	1.36	1.8	2	12	140
Phocid pinnipeds	0.75	1	2	1.9	30

Audiograms represent the auditory sensitivity of each species. However, to assess the impact of continuous anthropogenic noise, additional exposure metrics are required, namely, temporary threshold shift (TTS) and permanent threshold shift (PTS). These metrics define the cumulative sound exposure levels that can induce temporary or permanent auditory impairment in a given species. TTS and PTS are shown for every specie in Table 2.

To compare wind turbine noise with TTS and PTS criteria, the noise spectrum must be integrated over frequency and time assuming a continuous 24-h exposure. This integrated metric is the cumulative sound exposure level, $\mathrm{SEL}_{\mathrm{cum}}$. Prior to the integration, the source spectrum is weighted by a species-specific auditory weighting function $W(f)$, which represents the frequency-dependent hearing sensitivity of the species Table 3:

$$W(f) = C + \log_{10}\frac{(f/f_1)^{2a}}{(1+(f/f_1)^2)^a(1+(f/f_2)^2)^b}, \tag{9}$$

TABLE 4 | SEL_{CUM} for a single turbine and a squared 100-turbines layout for several functional hearing groups.

	Single turbine			100-turbine farm		
Hearing group	**NREL 5 MW**	**DTU 10 MW**	**EIA 22 MW**	**NREL 5 MW**	**DTU 10 MW**	**EIA 22 MW**
LF cetaceans	62.7	65.5	68.6	67.2	68.2	83.3
MF cetaceans	90.5	93.3	96.4	95.1	96.6	111.1
HF cetaceans	93.4	96.2	99.3	97.9	99.5	113.9
Phocid pinnipeds	70.5	73.3	76.4	75.1	76.6	91.2

where a, b, f_1, and f_2 are the fitted parameters shown in Table 3.

3 | Results and Discussion

Figure 5 shows the far-field aerodynamic noise spectra generated by a single wind turbine and a squared wind farm of 100 turbines, compared to the hearing thresholds of various functional hearing groups, that is, low-, mid-, and high-frequency cetaceans and pinnipeds [2, 38, 55]. The figure shows that aerodynamic noise from the three wind turbines affects the low-frequency hearing group even when considering only a single wind turbine.

When considering farms, Figure 5 shows that a group of 100 turbines causes a general increase in the amplitude of aerodynamic noise spectra. This increase is less significant for larger turbines due to the largest area occupied by the wind park (since we consider that the turbines are separated by 4.5D). Wind farms have an acoustic footprint underwater that is 9 dB louder than the hearing threshold of the Low-frequency functional hearing group for the case of the 5-MW wind turbine and 13 dB for the case of the 22-MW wind turbine. This underwater noise can potentially mask sounds used by marine animals for communication or interfere with natural ambient sounds in the environment.

Estimating the cumulative sound exposure level, SEL_{cum}, for offshore wind turbines is inherently uncertain, as it requires assuming that the turbine operates continuously at rated conditions over a full 24-h period. This assumption is rarely met in practice due to variability in wind conditions and turbine operation, and therefore the results presented here should be interpreted as a first-order estimate of potential exposure. Table 4 summarizes the SEL_{cum} obtained for each turbine type after applying the corresponding species-specific auditory weighting function.

For all functional hearing groups considered, the predicted exposure levels remain below commonly accepted thresholds for temporary threshold shift (TTS) and permanent threshold shift (PTS), indicating that no direct auditory injury is expected under the assumed conditions. Nevertheless, the computed levels exceed the hearing thresholds (audiograms) of the species, which implies that the turbine noise is audible and may lead to masking of biologically relevant sounds such as communication calls and echolocation signals. Consequently, even in the absence of physical hearing damage, ecological and behavioral impacts cannot be ruled out.

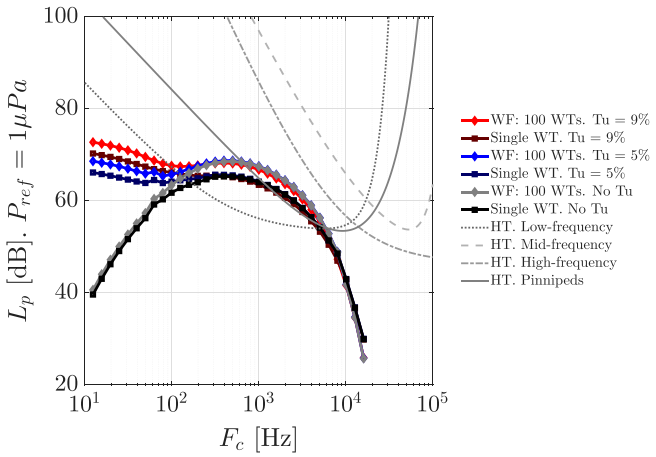

FIGURE 6 | Effect of the turbulence intensity on the aerodynamic noise generated by the IEA 22-MW wind turbine. Water-side observer (10 m deep) at 100 m downwind of the turbine. TE: trailing-edge noise; LE: leading-edge noise; Tu: turbulence intensity.

It is important to note that, in the case of wind farms, the resulting noise field depends strongly on the array layout, turbine spacing, bathymetry, and propagation conditions. Therefore, the simplified squared 100-turbine configuration considered here should not be regarded as representative of all developments, and the associated SEL_{cum} values should be interpreted with caution.

Having established a potential problem, we now focus on the largest turbine, the IEA 22-MW offshore turbine. The effect of inflow turbulence on the aerodynamic noise propagated underwater is shown in Figure 6. The same analyses have been conducted for the smaller turbines, showing similar results (not included for the sake of brevity). The results show that inflow turbulence noise significantly increases total aerodynamic noise in the frequency range up to 1 kHz. This increase is perceived by low- and mid-frequency cetacean hearing groups. Low-frequency noise is more critical as a result of its longer propagating distance underwater (larger wavelengths), which means that the acoustic footprint of the wind turbines is larger for lower frequencies. Therefore, turbulence intensity plays a role in the underwater aerodynamic noise of offshore wind turbines. However, the mechanical noise associated with the generator and radiated from the tower has a typical noise footprint for frequencies lower than 200 Hz and also needs to be considered to establish the dominance of LE noise of the total radiated noise of the wind turbine in this frequency range [13, 15, 16].

Our study shows that the main source of noise from offshore wind turbines that affects marine animals is produced by the trailing edge of the blade. The latter is produced at frequencies where marine animals have their highest hearing sensitivity (near the inflection point of the audiograms). Furthermore, trailing edge noise is generated for all operating conditions and does not depend on the inflow characteristics or mechanical components, making this source of noise more critical. This information should drive manufacturers and regulators to push for the inclusion of noise reduction techniques in offshore wind turbines, such as trailing-edge serrations [56], and consider noise emissions in optimization-related tasks [57].

Figure 7 compares the far-field noise for an Air-side observer (i.e., located on the air–water surface) and for a Water-side observer at 10-m depth (see Figure 3), at 100 and 500 m downstream the turbine. It is important to mention that for this case, the pressure reference for both observers is 1 μPa, which for the air is not the common reference pressure; however, this value is used just for comparison between both curves. For the Airside observer, noise is computed directly at the observer location for two conditions: including and neglecting atmosphere attenuation. The difference between the air-side and water-side observers is more pronounced at low frequencies. In this range, the blade sections radiate predominantly as dipole sources, yielding a relatively smooth directivity pattern that is only weakly sensitive to the propagation angle (approximately 13°). At higher frequencies, however, the radiation pattern becomes increasingly complex and exhibits multiple sidelobes. Consequently, the propagation angle becomes critical: Radiation at 13° may fall within a local minimum of the directivity pattern compared to the downstream direction of the air-side observer, leading to a substantially lower predicted level for the water-side receiver. In our formulation, the transmission coefficient at the air–water interface and the subsequent underwater propagation affect all frequencies in a similar manner. Therefore, the frequency-dependent differences observed between the air-side and water-side observers are primarily driven by source directivity rather than by transmission or underwater propagation effects. For receivers located further downstream, the refracted underwater wave becomes more parallel to the air–water interface (i.e., larger θ), which increases the transmission loss and further reduces the underwater sound pressure level. As a result, although the sound pressure level in air decreases with distance due to geometric spreading, the difference between the air-side and water-side observers increases with downstream distance, as shown in Figure 7.

Figure 7 shows that atmospheric attenuation causes a significant drop in far-field noise for frequencies higher than 1 kHz. If we also consider human hearing capacity (up to 20 kHz), then the aerodynamic noise of wind turbines is usually neglected at high frequencies (higher than 10 kHz). However, when considering underwater noise, the high-frequency range is less attenuated, and at the Water-side observer, the noise is louder than at the Air-side observer for frequencies higher than 5 kHz. This can be explained by direct airborne and indirect waterborne noise trajectories (see Section 2.2). For a Water-side observer, the sound wave travels through the air (medium with the highest attenuation) a maximum distance of $\approx (H+R)/\cos(13°)$, where H is the height of the hub and R is the wind turbine radius, which is much shorter than the distance from the source of the noise to an observer located downwind outside the water. This significantly reduces the atmospheric attenuation of the noise, which is more effective at higher frequencies. Furthermore, marine animals have hearing thresholds in a wider frequency range than humans; therefore, high frequencies are still relevant when analyzing marine environments.

Finally, we discuss the directivity pattern in the air and underwater. Figure 8a shows the directivity radiation pattern of a single IEA 22-MW wind turbine considering Air-side observers at a radius of 100 m for several centered frequencies (F_C) and the integrated overall sound pressure level (OSPL) over the entire frequency range. In air, the wind turbine radiates noise as a dipole aligned with the wind inflow with the lowest radiation amplitude on the rotor plane. Consequently, the selected Air-side observer in Figure 7 is aligned with the dipole main axis, whereas for the Water-side observer, only the noise that propagates underwater is the one near the rotor plane, following

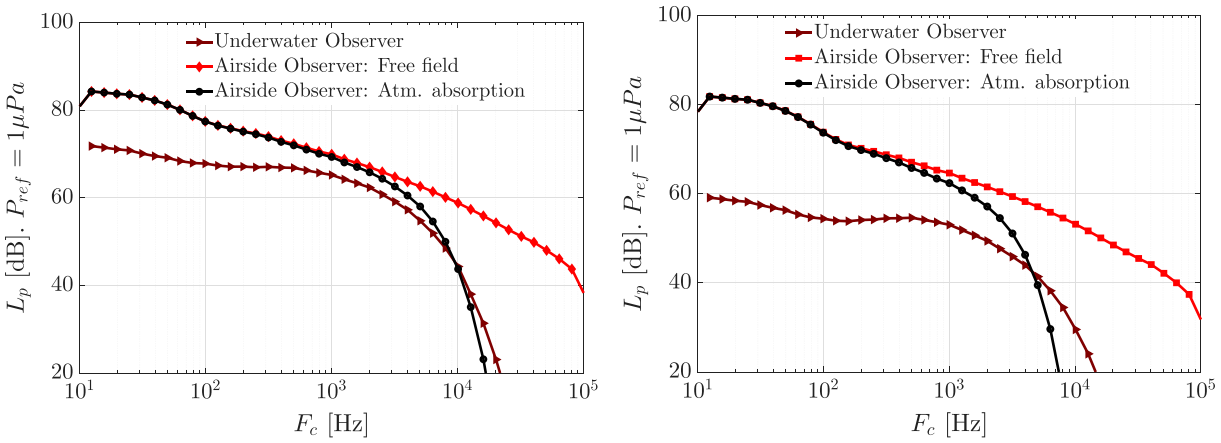

(a) 100 m downstream

(b) 500 m downstream

FIGURE 7 | IEA 22-MW wind turbine far-field noise prediction for a Water-side observer (10 m deep) and an Air-side observer at 500 m downwind of the turbine including (atm. attenuation) and neglecting (free field) atmospheric attenuation. (a) 100 m downstream. (b) 500 m downstream.

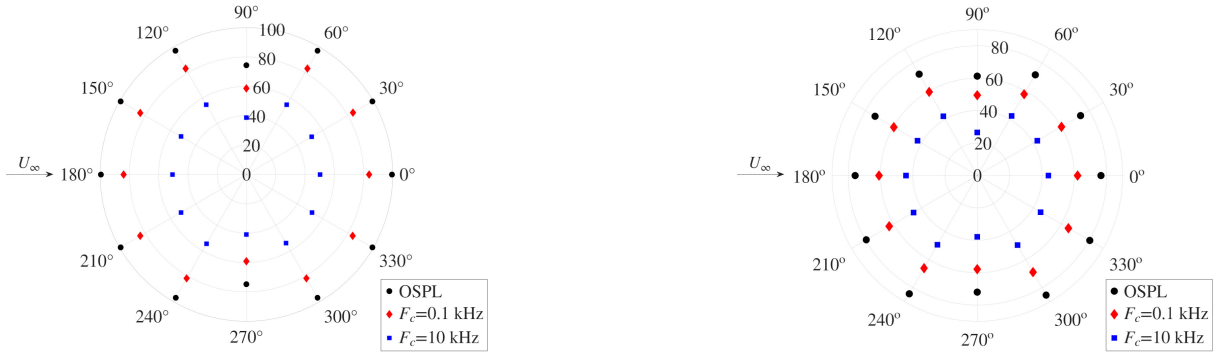

(a) Air-side directivity

(b) Water-side directivity

FIGURE 8 | Directivity pattern of a single IEA 22-MW wind turbine for Air-side and 10 m deep Water-side observers for several center frequencies and the overall sound pressure level (OSPL). (a) Air-side directivity. (b) Water-side directivity.

Snell's law. This also explains the lower noise radiated underwater than in air.

Figure 8b shows the directivity of the IEA 22-MW wind turbine at 10-m depth. Underwater, the turbine radiates noise with a dipole-like pattern aligned with the inflow velocity, consistent with the directivity observed in air. The overall azimuthal structure is preserved because the air–water interface modifies the propagation angle and amplitude (through refraction and transmission), but does not alter the underlying source directivity. However, the underwater dipole is not perfectly symmetric with respect to the inflow axis. Higher sound levels are observed in the lower half of the figure (from 180° to 360°), corresponding to the half-plane where the blades move downward. As reported by [18], blades radiate higher noise levels during the downward motion, which explains the asymmetry. In contrast, in air this asymmetry is less pronounced because the sound propagates directly to the observer without refraction at an interface, and the azimuthal symmetry of the dipole is therefore more clearly preserved.

4 | Conclusions and Future Works

The environmental impacts of offshore energy devices must be carefully considered to achieve truly sustainable energy exploitation. A major concern with offshore wind turbines is underwater noise, which can negatively affect marine species. So far, turbine design for offshore environments has prioritized energy production, often neglecting its acoustic footprint. In particular, the aerodynamic noise transmitted underwater remains unquantified.

In this study, we have presented a methodology for predicting underwater aerodynamic noise from wind turbines by integrating existing noise prediction models with wave propagation theory. This methodology is a breakthrough for manufacturers and policymakers in quantifying the environmental impact of wind energy devices related to noise emissions. The methodology shows a straightforward implementation for low-fidelity models used in optimization-related techniques or regulations. However, it can be easily coupled with high-fidelity methods to characterize the noise source (flow) or the noise propagation.

For the first time, we have quantified the underwater aerodynamic acoustic footprint of three large offshore wind turbines—5, 10, and 22 MW—as well as an array of 100 turbines. The predicted radiated noise levels were compared with published marine species' audiograms and available temporary threshold shift criteria. The results indicate that aerodynamic noise is transmitted across the air-sea interface and may be detectable by several marine species over a broad frequency range, suggesting a possible contribution to masking of biologically relevant sounds. For the conditions considered in this study, the predicted levels remain below temporary threshold shift for the species examined. The analysis further suggests that underwater aerodynamic noise levels increase with turbine size, turbulence intensity, and the number of turbines in an array. These findings highlight the importance of considering aerodynamic noise in future environmental assessments of large offshore wind farms and suggest that existing noise-reduction strategies developed for onshore turbines (e.g., serrated trailing edges) could also be explored in the offshore context.

To implement the methodology proposed in real scenarios, three additions can be considered. The state of the sea, that is, waves, needs to be considered to replace the flat-interface assumption. This would potentially influence the direction of the noise generation (Snell cone), as Φ would change according to the angle of the wave. The other consideration is the background noise from the underwater wind farm. If available, the latter can be overlaid on the proposed spectra to confirm whether the noise generated by the wind turbines is audible by the marine animals (and not masked by the background noise). To calculate a most precise SEL_{cum} a operational histogram over 24-h should be considered. Finally, to more accurately predict the wind farm noise, a specific layout and acoustic observer need to be provided. Furthermore, wake-resolved simulations could be performed to calculate the influence of wake in the generation and propagation of noise.

Author Contributions

Laura Botero-Bolívar: conceptualization, data curation, formal analysis, investigation, methodology, software, validation, visualization,

writing – original draft. **Oscar A. Marino Sánchez:** investigation, methodology, validation, writing – review and editing. **Martín de Frutos:** investigation, methodology, validation, writing – review and editing. **Esteban Ferrer:** conceptualization, methodology, validation, funding acquisition, project administration, resources, supervision, writing – review and editing.

Acknowledgments

This research has received funding from the European Union (ERC, Off-coustics, project number 101086075). Also, the authors acknowledge the support of Universidad Industrial de Santander (project number 4632, "METODOLOGÍA DE PREDICCIÓN RÁPIDA DEL RUIDO SUBMARINO EN TURBINAS EÓLICAS Y MAREOMOTRICES Y SUS ARREGLOS") and the Energy and Environment research group (GIEMA). Views and opinions expressed are, however, those of the authors only and do not necessarily reflect those of the European Union or the European Research Council. Neither the European Union nor the granting authority can be held responsible for them.

Funding

This research has received funding from the European Union (ERC, Off-coustics, project number 101086075). Also, the authors acknowledge the support of Universidad Industrial de Santander (project number 4632, "METODOLOGÍA DE PREDICCIÓN RÁPIDA DEL RUIDO SUBMARINO EN TURBINAS EÓLICAS Y MAREOMOTRICES Y SUS ARREGLOS") and the Energy and Environment research group (GIEMA).

Conflicts of Interest

The authors declare no conflicts of interest.

Data Availability Statement

The data that support the findings of this study are available from the corresponding author, Botero-Bolívar, L., upon reasonable request. Furthermore, the algorithm to predict wind turbine noise is available in [58].

References

1. T. Götz, G. Hastie, L. Hatch, et al., "Overview of the Impacts of Anthropogenic Underwater Sound in the Marine Environment," (2009), OSPAR Commission.

2. C. Erbe, C. Reichmuth, K. Cunningham, K. Lucke, and R. Dooling, "Communication Masking in Marine Mammals: A Review and Research Strategy," *Marine Pollution Bulletin* 103 (2016): 15–38.

3. U. Stöber and F. Thomsen, "How Could Operational Underwater Sound From Future Offshore Wind Turbines Impact Marine Life?," *Journal of the Acoustical Society of America* 149, no. 3 (2021): 1791–1795.

4. J. N. Daly and J. Harrison, "The Marine Mammal Protection Act: A Regulatory Approach to Identifying and Minimizing Acoustic-Related Impacts on Marine Mammals," in *The Effects of Noise on Aquatic Life* (Springer New York, 2012), 537–539.

5. J. Tougaard, L. Hermannsen, and P. T. Madsen, "How Loud Is the Underwater Noise From Operating Offshore Wind Turbines?," *Journal of the Acoustical Society of America* 148 (2020): 2885–2893.

6. N. Akhtar, B. Geyer, and C. Schrum, "Larger Wind Turbines as a Solution to Reduce Environmental Impacts," *Nature Scientific Reports* 14, no. 1 (2024): 6608, https://doi.org/10.1038/s41598-024-56731-w.

7. P. Sherman, X. Chen, and M. McElroy, "Offshore Wind: An Opportunity for Cost-Competitive Decarbonization of China's Energy Economy," *Science Advances* 6, no. 8 (2020): eaax9571, https://doi.org/10.1126/sciadv.aax9571.

8. B. Desalegn, D. Gebeyehu, B. Tamrat, T. Tadiwose, and A. Lata, "Onshore Versus Offshore Wind Power Trends and Recent Study Practices in Modeling of Wind Turbines Life-Cycle Impact Assessments," *Cleaner Engineering and Technology* 17 (2023): 100691, https://www.sciencedirect.com/science/article/pii/S2666790823000964.

9. F. Zahle, A. Barlas, K. Lønbæk, et al., "*Definition of the IEA Wind 22-Megawatt Offshore Reference Wind Turbine*," (Technical University of Denmark, 2024).

10. Mingyang-Wind-Power, "Myse 22 MW From Mingyang Wind Power," (2024), https://www.myse.com.cn/en/wind-turbine/index.aspx.

11. Orsted, "Hornsea 1 Offshore Wind Farm," (2024), Accessed: 2024-10-01.

12. C. Hooper, J. Nedwell, D. J. Nedwell, M. J. Langworthy, and M. D. Howell, "Assessment of Sub-Sea Acoustic Noise and Vibration From Offshore Wind Turbines and Its Impact on Marine Wildlife; Initial Measurements of Underwater Noise during Construction of Offshore Windfarms, and Comparison With Background Noise," (2003), https://www.subacoustech.com.

13. P. T. Madsen, M. Wahlberg, J. Tougaard, K. Lucke, and P. Tyack, "Wind Turbine Underwater Noise and Marine Mammals: Implications of Current Knowledge and Data Needs," *Marine Ecology Progress Series* 309 (2006): 279–295.

14. M. Marini, R. Baccoli, C. C. Mastino, A. D. Bella, C. Bernardini, and M. Masullo, "Assessment of the Noise Generated by Wind Turbines at Low Frequencies," *Journal of Energy Resources Technology, Transactions of the ASME* 139 (2017).

15. F. Thomsen and R. Kafemann, "Effects of Offshore Wind Farm Noise on Marine Mammals and Fish," (2006), https://www.offshorewind.co.uk.

16. J. Tougaard, O. D. Henriksen, and L. A. Miller, "Underwater Noise From Three Types of Offshore Wind Turbines: Estimation of Impact Zones for Harbor Porpoises and Harbor Seals," *Journal of the Acoustical Society of America* 125 (2009): 3766–3773.

17. D. M. F. Chapman and P. D. Ward, "The Normal-Mode Theory of Air-to-Water Sound Transmission in the Ocean," *Journal of the Acoustical Society of America* 87 (1990): 601–618.

18. S. Oerlemans, P. Sijtsma, and B. Méndez López, "Location and Quantification of Noise Sources on a Wind Turbine," *Journal of Sound and Vibration* 299, no. 4 (2007): 869–883.

19. R. Schlinker and R. Amiet, "Helicopter Rotor Trailing Edge Noise," in *7th Aeroacoustics Conference*, (1981), 2001.

20. R. K. Amiet, "Acoustic Radiation From an Airfoil in a Turbulent Stream," *Journal of Sound and Vibration* 41, no. 4 (1975): 407–420.

21. R. K. Amiet, "Noise Due to Turbulent Flow Past a Trailing Edge," *Journal of Sound and Vibration* 47, no. 3 (1976): 387–393.

22. M. Roger and S. Moreau, "Back-Scattering Correction and Further Extensions of Amiet's Trailing-Edge Noise Model. Part 1: Theory," *Journal of Sound and Vibration* 286, no. 3 (2005): 477–506.

23. T. von Kármán, "Progress in the Statistical Theory of Turbulence," *Proceedings of the National Academy of Sciences* 34, no. 11 (1948): 530–539.

24. O. Stalnov, P. Chaitanya, and P. F. Joseph, "Towards a Non-Empirical Trailing Edge Noise Prediction Model," *Journal of Sound and Vibration* 372 (2016): 50–68.

25. M. Drela, "Xfoil: An Analysis and Design System for Low Reynolds Number Airfoils," *Low Reynolds Number Aerodynamics* 54 (1989): 1–12.

26. P. Bortolotti, M. Masciola, S. Ananthan, et al., "Openfast," (2022), https://github.com/OpenFAST/openfast/tree/v3.1.0.

27. Y. Tian and B. Cott, "Wind Turbine Noise Modeling Based on Amiet's Theory: Effects of Wind Shear and Atmospheric Turbulence," *Acta Acustica united with Acustica* 102 (2016): 626–639.

28. E. Barlas, W. J. Zhu, W. Z. Shen, K. O. Dag, and P. Moriarty, "Consistent Modelling of Wind Turbine Noise Propagation From Source to Receiver," *Journal of the Acoustical Society of America* 142, no. 5 (2017): Article 3297.

29. S. Oerlemans and J. G. Schepers, "Prediction of Wind Turbine Noise and Validation Against Experiment," (2009), Nationaal Lucht-en Ruimtevaartlaboratorium (NLR) / National Aerospace Laboratory, NLR-TP-2009-402.

30. P. Moriarty and P. Migliore, "Semi-Empirical Aeroacoustic Noise Prediction Code for Wind Turbines," (2003), Technical Report, National Renewable Energy Laboratory, Golden, CO, USA, NREL/TP-500-34478.

31. L. Botero-Bolívar, O. A. Marino, C. H. Venner, L. D. de Santana, and E. Ferrer, "Low-Cost Wind Turbine Aeroacoustic Predictions Using Actuator Lines," *Renewable Energy* 227 (2024).

32. Z. Sun, W. Zhu, E. Jan, X. Wang, W. Z. Shen, and E. Ferrer, "Sound Propagation Analysis of a 10 MW Wind Turbine: Influence of the Tower, Operational States, and Atmospheric Conditions," *Renewable Energy* 255 (2025): 123842, https://www.sciencedirect.com/science/article/pii/S096014812501506X.

33. A. P. Bresciani, B. Kale, L. Botero-Bolivar, J. Christophe, and C. Schram, "Benchmarking Wind Turbine Noise Predictions in Real Weather Conditions," in *30th AIAA/CEAS Aeroacoustics Conference (2024)*, (2024), 3193.

34. D. M. F. Chapman, D. J. Thomson, and D. D. Ellis, "Modeling Air-to-Water Sound Transmission Using Standard Numerical Codes of Underwater Acoustics," *Journal of the Acoustical Society of America* 91 (1992): 1904–1910.

35. Y. Chen, *Spherical Wave Reflection and Transmission*, (Open University (United Kingdom), 1992).

36. C. H. Hansen, C. J. Doolan, and K. L. Hansen, *Wind Farm Noise: Measurement, Assessment, and Control*, (2017).

37. A. A. Hudimac, "Ray Theory Solution for the Sound Intensity in Water Due to a Point Source Above It," *Journal of the Acoustical Society of America* 29, no. 8 (1957): 916–917.

38. C. Carter, B. Wilson, and M. Burrows, "Tidal Energy Underwater Noise and Marine Mammals," (2013), PhD Thesis.

39. ANSI/ASA, "ANSI/ASA S1. 26-2014: Methods for Calculation of the Absorption of Sound by the Atmosphere," (2014), American National Standards Institute Melville, NY.

40. F. H. Fisher and V. P. Simmons, "Sound Absorption in Sea Water," *Journal of the Acoustical Society of America* 62, no. 3 (1977): 558–564.

41. J. Jonkman, S. Butterfield, W. Musial, and G. Scott, "Definition of a 5-MW Reference Wind Turbine for Offshore System Development," (2009), National Renewable Energy Laboratory, https://www.nrel.gov/docs/fy09osti/38060.pdf.

42. C. Bak, R. Bitsche, A. Yde, et al., "*Light Rotor: The 10-MW Reference Wind Turbine*," (2012), http://events.ewea.org/annual2012/.

43. F. Zahle, T. Barlas, K. Lønbæk, et al., *IEAWINDTASK37/IEA-22-280-RWT: v1.0.1*, (Zenodo, 2024), https://doi.org/10.5281/zenodo.10944127.

44. B. Kale, "ABL Simulations With Uncertain Weather Parameters and Impact on WT Performance and Near-Field Noise," (2023), PhD Thesis.

45. M. Türk and S. Emeis, "The Dependence of Offshore Turbulence Intensity on Wind Speed," *Journal of Wind Engineering and Industrial Aerodynamics* 98 (2010): 466–471.

46. B. L. Southall, A. E. Bowles, W. T. Ellison, et al., "Marine Mammal Noise Exposure Criteria: Initial Scientific Recommendations," *Aquatic Mammals* 33, no. 4 (2007): 411–521.

47. B. L. Southall, J. J. Finneran, C. Reichmuth, et al., "Marine Mammal Noise exposure Criteria: Updated Scientific Recommendations for Residual Hearing Effects," *Aquatic Mammals* 45, no. 2 (2019): 125–232.

48. National Marine Fisheries Service, "Technical Guidance for Assessing the Effects of Anthropogenic Sound on Marine Mammal Hearing (Version 3.0)," (2024), U.S. Department of Commerce, NOAA.

49. C. S. Johnson, "Sound Detection Thresholds in Marine Mammals," *Marine Bioacoustics* 1967 (1967): 247–260.

50. R. A. Kastelein, P. Bunskoek, M. Hagedoorn, W. W. L. Au, and D. de Haan, "Audiogram of a Harbor Porpoise Measured With Narrow-Band Frequency-Modulated Signals," *Journal of the Acoustical Society of America* 112, no. 1 (2002): 334–344.

51. D. Kastak and R. J. Schusterman, "Low-Frequency Amphibious Hearing in Pinnipeds: Methods, Measurements, Noise, and Ecology," *Journal of the Acoustical Society of America* 103, no. 4 (1998): 2216–2228.

52. J. M. Terhune, "Masked and Unmasked Pure Tone Detection Thresholds of a Harbour Seal Listening in Air," *Canadian Journal of Zoology* 69, no. 8 (1991): 2059–2066.

53. C. E. Schlundt, J. J. Finneran, D. A. Carder, and S. H. Ridgway, "Temporary Shift in Masked Hearing Thresholds of Bottlenose Dolphins and White Whales After Exposure to Intense Tones," *Journal of the Acoustical Society of America* 107, no. 6 (2000): 3496–3508.

54. D. S. Houser and J. J. Finneran, "Comparison of Underwater Hearing Sensitivity in Bottlenose Dolphins and Humans," *Journal of the Acoustical Society of America* 123, no. 5 (2008): 2980–2992.

55. J. Tougaard, "Thresholds for Noise Induced Hearing Loss in Marine Mammals," *Journal of Aeroacoustics Society of America* 118 (2021): 3154–3163.

56. S. Oerlemans, "Reduction of Wind Turbine Noise Using Blade Trailing Edge Devices," in *22nd AIAA/CEAS Aeroacoustics Conference*, (2016), 3018.

57. M. de Frutos, O. A. Marino, D. Huergo, and E. Ferrer, "Deep Reinforcement Learning for Multi-Objective Optimization: Enhancing Wind Turbine Energy Generation While Mitigating Noise Emissions," (2024), https://arxiv.org/abs/2407.13320.

58. L. Botero-Bolívar, "Wind Turbine Noise Prediction," (2023), https://github.com/lauraboterob/WindTurbine_Noise_prediction.

59. G. Leloudas, "Optimization of Wind Turbines With Respect to Noise," (2006), Master's Thesis, Technical University of Denmark, Anker Engelunds Vej 1, Building 101A, 2800 Kgs. Lyngby.

60. J. Christophe, S. Buckingham, C. Schram, and S. Oerlemans, "Zephyr—Large on Shore Wind Turbine Benchmark," (2022), Zenodo, https://doi.org/10.5281/zenodo.7323750.

Appendix A

Representation of Acoustic Ray Refraction and Calculation of Snell's Angles

Figure A1 shows the geometric representation in 2D of an acoustic ray connecting a single noise source with a receptor. Based on the triangles formed by the acoustic ray in the air and in the water.

The incident and refracted angles (Φ and θ, respectively) are obtained by solving the following system of equations:

$$\begin{aligned} l &= h\tan(\Phi) + d\tan(\theta) \\ c_w \sin(\Phi) &= c_a \sin(\theta). \end{aligned} \tag{A1}$$

The first equation expresses the horizontal distance between the noise source and the Water-observer in terms of the source height h, the observer depth d, and the tangents of the incident and refracted angles. The second equation corresponds to Snell's law, which relates both angles through the ratio of sound speeds in water (c_w) and air (c_a). Physically, this system determines the ray geometry connecting source and observer across the air–water interface. To avoid complex-valued solutions of the nonlinear system, the refracted angle θ is obtained with the geometrical constraint $\theta = \tan^{-1}((l - h\tan(\Phi))/d)$ and the obtained solution is accepted only if it satisfies Snell's law within a tolerance of 10^{-2}. Figure A1 shows a 2D representation of the variables here presented.

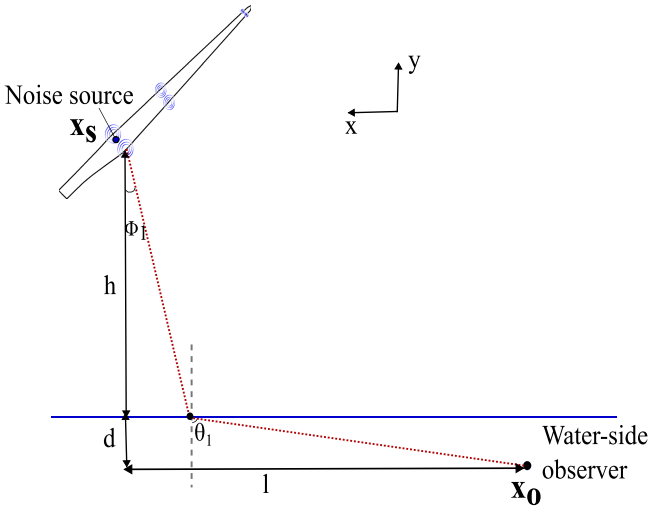

FIGURE A1 | Geometric representation of acoustic ray following Snell's law. X_s is the vectorial location of the noise source and X_o is the vectorial location of the Water-side observer.

Appendix B

Algorithm of Wind Turbine Noise Prediction at the Water-Side Observer

Figure B1 shows the algorithm to calculate the aerodynamic wind turbine noise at the Water-side observer.

Appendix C

Transmission Loss at the Air–Water Interface Calculated Using Planar and Spherical Waves Theory

Planar wave theory is the simplest model that we can use to model the transmission loss at the air–water interface. This model can introduce some inaccuracies at low-frequencies and when the noise source is relatively close to the interface. We have demonstrated that in the cases used in this research, we can consider sound waves as planar because $\lambda/r > 10$ (see Figure 4). In this Appendix, we will discuss the effect of calculating the transmission loss with the spherical wave propagation model.

The analytical expression for the transmission loss of the pressure ($T_{a\to w}$) for spherical and planar waves for two fluid media is defined as [35]:

Spherical waves:

$$T_{a\to w} = \frac{\phi_{in}\rho_2}{\phi_{out}\rho_1}; \tag{C1}$$

where ϕ_{in} and ϕ_{out} are incident and transmitted pressure waves, and ρ_1 and ρ_2, the density of the two mediums (in our case air and water). The incident and transmitted pressure waves are

$$\phi_{in} = \int_0^\infty \frac{J_0(r_i x)}{q_1} e^{-|z-h|q_1} x\,dx, \tag{C2}$$

$$\phi_{out} = \int_0^\infty T \cdot \frac{J_0(r_i x)}{q_2} e^{-hq_1+zq_2} x\,dx; \tag{C3}$$

where $r = h\tan(\theta)$, h is the height of the noise source, $z = 0$ is the location of the interface, and T is the transmission coefficient defined as

$$T = \frac{2\rho_1 q_2}{\rho_2 q_1 + \rho_1 q_2}; \tag{C4}$$

where $q_1 = \sqrt{1-\kappa_1^2}$ and $q_1 = \sqrt{1-\kappa_1^2}$, and κ_1 and κ_2 are the wavenumber ($\kappa = 2\pi f/c$) of medium 1 and 2, respectively (c the speed of sound of each medium). Next, we detail the transmission loss for planar waves.

Planar waves:

$$T_{a\to w} = T\frac{\rho_2}{\rho_1}; \tag{C5}$$

where T is defined as

$$T = \frac{2\rho_1\cos\Phi}{\rho_2\cos\Phi + \rho_1\sqrt{\frac{c_1^2}{c_2^2} - \sin^2\Phi}}. \tag{C6}$$

Substituting Equation (C6) in Equation (C5) results in $T_{a\to w} = \frac{2\cos(\Phi)}{\cos(\Phi)+gn\cos(\theta)}$, presented in Equation (4), where $g = \rho_1/\rho_2$ and $n = c_1/c_2$.

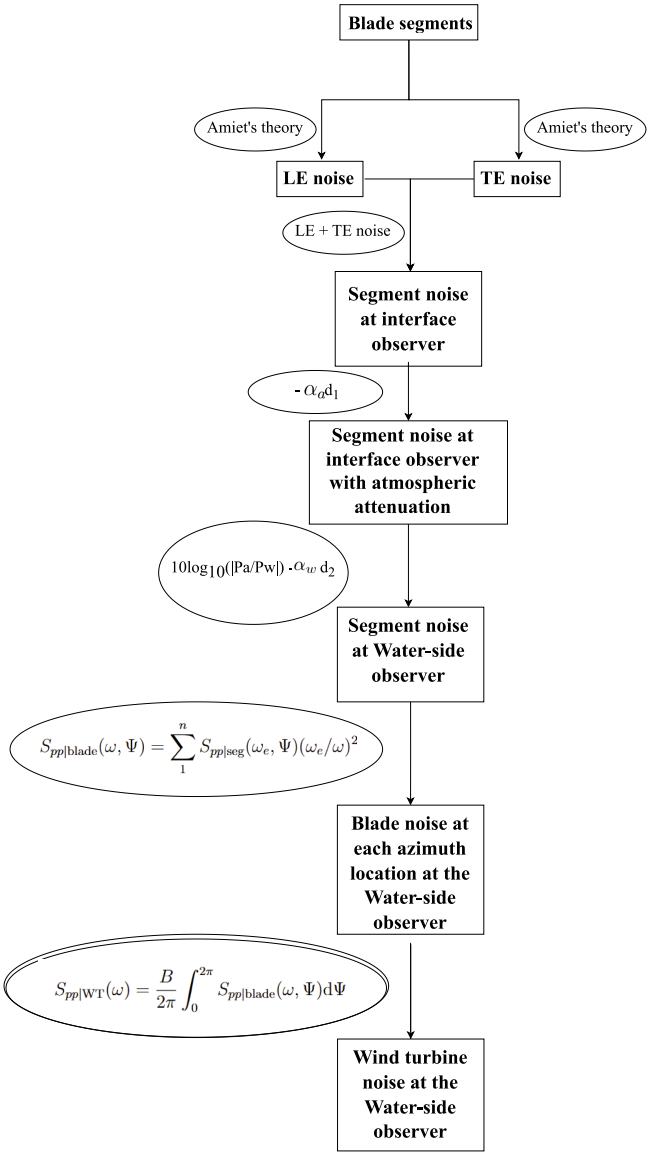

FIGURE B1 | Algorithm for the wind turbine noise prediction at the Water-side observer.

The transmission loss of the sound intensity (for either implementation) can be calculated as $T_i = 10\log_{10}\left(|T_p|^2 \frac{Z_1}{Z_2}\right)$, where Z_1 and Z_2 are the impedance ($Z = \rho c$) of each medium.

Figure C1 shows the loss of sound intensity transmission for spherical and plane waves for several frequencies at two heights of the noise source, that is, 90 and 170 m, which are the hub heights of the shortest and tallest turbines that we study in our manuscript. The figure shows that the transmission loss for the spherical wave fluctuates along the angle of incidence, whereas the plane wave loss remains flat. What is important here is that the difference between the plane and spherical losses is not larger than 1.5 dB (for any incident angle). More specifically, at $\theta = 13.1°$, that is, the critical Snell angle for air and water, the difference is less than 0.5 dB.

To verify our previous results, we have coupled the spherical wave transmission loss with our proposed prediction method. The results are shown in Figure C2. It can be seen that there is no difference in the far-field noise spectrum when switching from plane wave theory to spherical plane for the wind turbine application at hand.

For completeness, Figure C3 shows the difference in the average transmission loss calculated with spherical and planar wave theory, throughout the frequency range and for each blade section at each azimuth location for both, the EIA 22 MW and the NREL 5 MW, the largest and smallest turbines, respectively. The difference in transmission loss is less than 0.6 dB for all the frequencies and sections.

Appendix D

Validation of Noise Prediction Method

The test case for noise prediction validation is the Siemens SWT-2.3-93 wind turbine, which is a three-blade horizontal axis wind turbine located in the Høvsøre Wind Turbine Test Center in the northwest of Denmark. It has a nominal rated power of 2.3 MW. The rotor diameter is 93 m, and the hub height is 80 m.

Noise measurements at various operating conditions are reported in [59]. The acoustic and met-mast measurements, operational curves, and wind turbine CAD are available in the database [60]. We use the described methodology to compute the wind turbine noise for the two operational conditions summarized in Table D1. The inflow turbulence conditions at the hub height are calculated from atmospheric LES simulations reported in [44] for one specific operational condition. Note that the same turbulence parameters are used for other operational conditions, assuming that the atmospheric turbulence does not vary

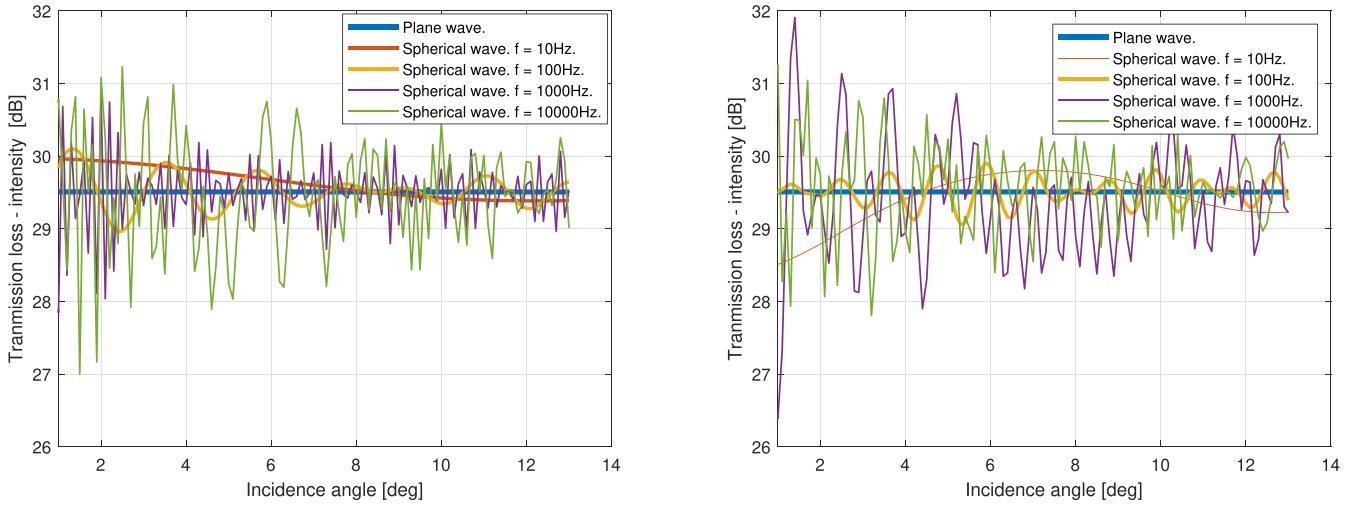

(a) Distance from source to sea level: h = 90 m

(b) Distance from source to sea level: h = 170 m

FIGURE C1 | Intensity transmission loss as a function of the incidence angle for several distances (source to sea level) and frequencies. (a) Distance from source to sea level: h = 90 m. (b) Distance from source to sea level: h = 170 m.

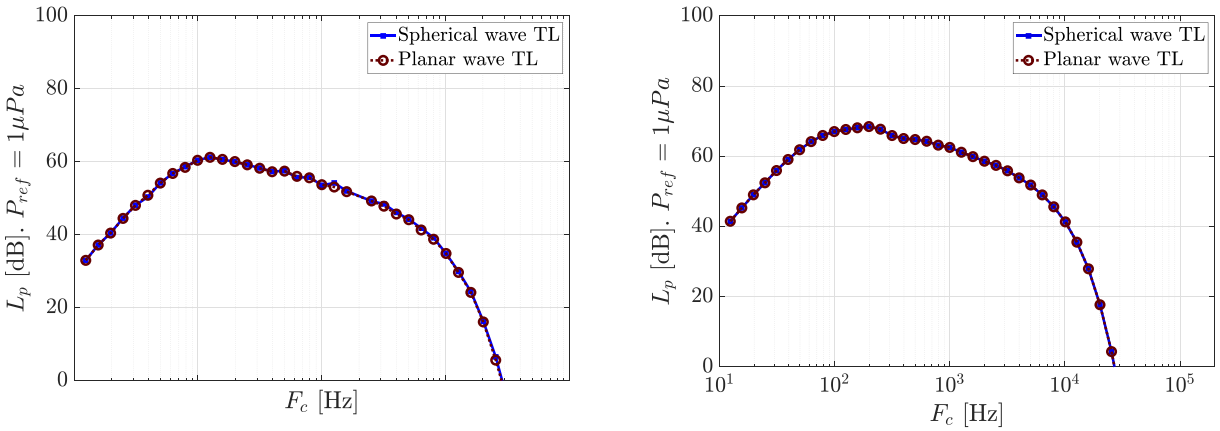

(a) NREL 5 MW

(b) IEA 22 MW

FIGURE C2 | Wind turbine trailing-edge noise for an observer located 100 m downstream and 10 m underwater obtained with spherical and planar wave transmission loss (to account for the change in media). (a) NREL 5 MW. (b) IEA 22 MW.

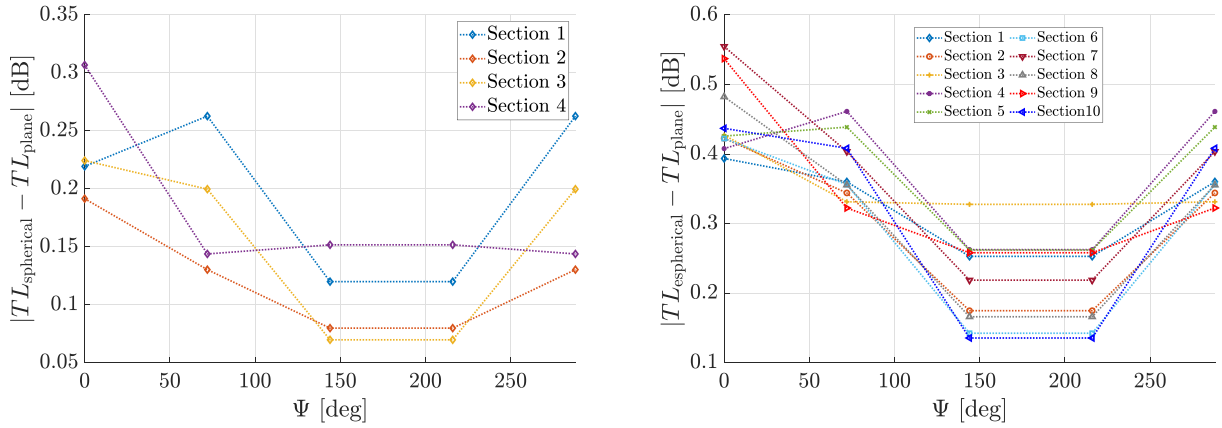

(a) IEA 22 MW (b) NREL 5 MW

FIGURE C3 | Average difference in the intensity transmission loss along the frequency range calculated with spherical and plane wave theories for each blade section at each azimuth location. (a) IEA 22 MW. (b) NREL 5 MW.

TABLE D1 | Operational conditions of the Siemens SWT-2.3-93 wind turbine.

Operational condition	U_∞ (m/s)	Ω (rpm)	θ (deg)
O.C. 1	9.5	17	5
O.C. 2	6.0	13	3

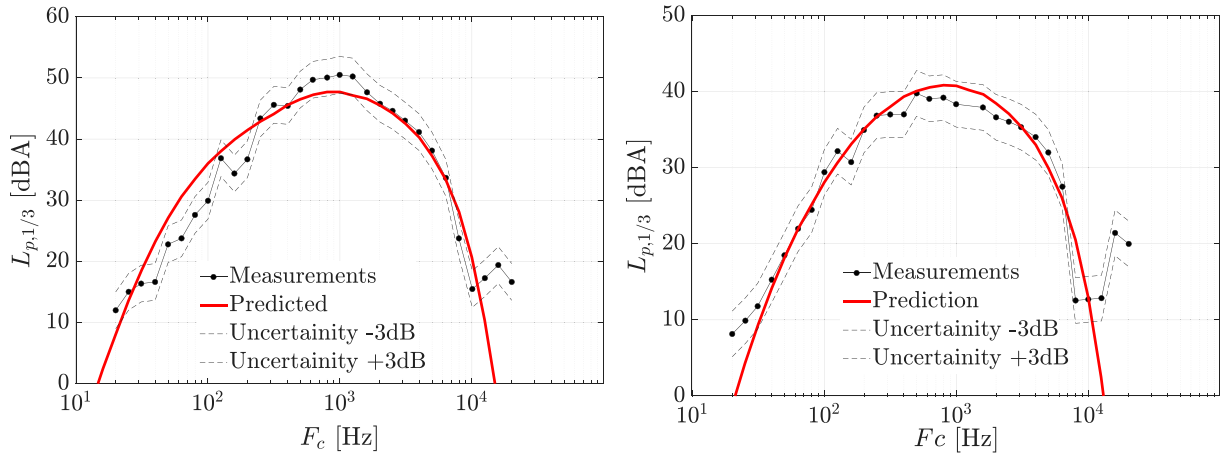

(a) Operational condition 1. (b) Operational condition 2.

FIGURE D1 | Predicted and measured wind turbine far-field noise for several operational conditions shown in Table D1. (a) Operational condition 1. (b) Operational condition 2.

significantly with the wind speed. The turbulence intensity and turbulence integral length scale at the hub height, needed to predict LE noise, are $Tu_\infty = 10.7\%$, and $L = 300$ m. The noise is measured at the ground at 100 m downwind of the wind turbine.

It is worth noting that, although the validation results are very similar to those presented in previous work, the predictions shown here are obtained using the same methodology applied to the other turbines analyzed in this study, namely, BEMT aerodynamic loading computed with OpenFAST and coupled with Amiet's theory for noise prediction. This ensures methodological consistency throughout the manuscript.

Figure D1 shows the comparison of the predicted wind turbine noise with the measurements reported in [59]. For both operational conditions, the wind turbine noise prediction agrees well with field measurements; predictions are between the uncertainty curves in the frequency range from 100 Hz up to $f \approx 20$ kHz. This good agreement provides important validation to the methodology presented in this research including, wall-pressure spectrum method, XFOIL simulation, and inflow turbulence spectrum.